



3D bioprinted hyaluronic acid-based cell-laden scaffold for brain microenvironment simulation

Liang Ma^{1,2} · Yuting Li^{1,2} · Yutong Wu^{1,2} · Mengfei Yu³ · Abdellah Aazmi^{1,2} · Lei Gao^{1,2} · Qian Xue^{1,2} · Yichen Luo^{1,2} · Hongzhao Zhou^{1,2} · Bin Zhang^{1,2} · Huayong Yang^{1,2}

Received: 9 April 2020 / Accepted: 27 April 2020 / Published online: 13 May 2020
© Zhejiang University Press 2020

Abstract

Treatments for lesions in central nervous system (CNS) are always faced with challenges due to the anatomical and physiological particularity of the CNS despite the fact that several achievements have been made in early diagnosis and precision medicine to improve the survival and quality of life of patients with brain tumors in recent years. Understanding the complexity as well as role of the microenvironment of brain tumors may suggest a better revealing of the molecular mechanism of brain tumors and new therapeutic directions, which requires an accurate recapitulation of the complex microenvironment of human brain *in vitro*. Here, a 3D bioprinted *in vitro* brain matrix-mimetic microenvironment model with hyaluronic acid (HA) and normal glial cells (HEBs) is developed which simulates both mechanical and biological properties of human brain microenvironment *in vivo* through the investigation of the formulation of bioinks and optimization of printing process and parameters to study the effects of different concentration of gelatin (GA) within the bioink and different printing structures of the scaffold on the performance of the brain matrix-mimetic microenvironment models. The study provides experimental models for the exploration of the multiple factors in the brain microenvironment and scaffolds for GBM invasion study.

Keywords 3D microextrusion bioprinting · Hyaluronic acid · GBM invasion model · Brain matrix-mimetic

Introduction

Understanding the extremely complex human brain microenvironment is crucial for brain tumor study as well as development of therapeutic drugs because of the huge threat of

brain tumors to people's health worldwide. To be specific, malignant gliomas remain deadly and glioblastoma multiforme (GBM), the most malignant type, frequently kills patients within a year of diagnosis. Even with modern medical treatment such as neuro-surgery or radiation therapy, the 5-year survival rate is still miserable and lower than 5% [1]. The invasive growth feature of GBM is the main cause that is responsible for the high recurrence rate, high mortality and poor clinical efficacy [2]. Recently, investigations have found out the tumor microenvironment; especially ECMs play a key role in the GBM progression and invasion [3, 4]; however, the underlying molecular mechanism is still not clear. Thus, creating tumor *in vitro* models can be a possible way to study the interactions between the tumor-related cells and surrounding ECM molecules, which requires simulations of brain microenvironment in the form of hydrogel scaffolds laden with normal brain cells in the first place.

Besides the applications of *in vitro* brain microenvironment in brain tumor study, there are also prominent demands for *in vitro* tumor microenvironment constructions to investigate the biological features as well as effective therapeutic treatments of multiple types of tumor. In recent decades,

Liang Ma and Yuting Li have contributed equally to this work.

✉ Liang Ma
liangma@zju.edu.cn

✉ Hongzhao Zhou
hz_zhou@zju.edu.cn

✉ Bin Zhang
zbxzju@zju.edu.cn

¹ State Key Laboratory of Fluid Power and Mechatronic Systems, Zhejiang University, Hangzhou 310058, People's Republic of China

² School of Mechanical Engineering, Zhejiang University, Hangzhou 310058, People's Republic of China

³ The Affiliated Stomatologic Hospital, School of Medicine, Zhejiang University, Hangzhou 310003, People's Republic of China

in vitro tumor models [5] were proved to be powerful tools for fundamental biological studies [6, 7] to explore the cross-talk between the tumor and ECM [8] or cell–cell interactions [9] and further as platforms for anticancer drug screening [10]. Conventional tissue engineering has been used to build multiple tumor models [11] and organs-on-chips [12] in the past decades; the shortcomings of these methods have been gradually revealed including the lack of controllable spatial distribution of different cell types and extracellular components, which makes it difficult for those models in vitro to precisely mimic the progression and development of the organs and tumors involved. In addition, methods from tissue engineering always fail to build models with relatively large scale and complex structures [13]. Until recently, 3D bioprinting has been introduced to create tumor in vitro models with its advantages which can precisely control the cell's spatial distribution and able to realize the heterogeneous feature of tumors [14]. With the excellent ability to distribute multiple components of the environment with defined location and structure, 3D bioprinting has been extensively used in the past decade to model multiple tissues/organs and diseases [15]. This emerging biofabrication technique enables the construction of in vitro 3D tumor models [16] with high resolution and throughput [17]. The most important advantage of 3D bioprinting is the ability to construct models with extremely complex and elaborate structures and biological components. Also, different 3D bioprinting strategies such as inkjet, extrusion, laser-based and photocuring bioprinting are available for different bioinks and demands [18]. More recently, this versatile technique has further found its application in studying cancer genesis, progression, metastasis [19] and drug responses [20] through the creation of accurate models that reproduce the complexity of the cancer microenvironment [21, 22].

When it comes to 3D bioprinted brain tissues, most of the efforts up to now are about glioma in vitro models focused on investigation of the molecular mechanism of the tumor and some of them could be used for therapeutic research and drug screening. Heinrich and other coworkers printed mini-brain consisting of glioblastoma cells and macrophages which was presented as a useful tool to study the interactions between these two cell types and to test therapeutics that target this interaction [23]. Dai et al. [24] conducted a research on a 3D bioprinted glioma stem cell model with high viability and inherent characteristics of the cells to mimic the microenvironment of brain tumor and found out that glioma stem cells expressed several biomarkers and showed potential functions and more resistance to chemotherapeutics (TMZ) compared with 2D condition. Later, the research team fabricated self-assembled multicellular heterogeneous brain tumor fibers with a coaxial extrusion 3D bioprinting system to study the interaction between tumor cells and stromal cells and provided an optimized platform to research

tumor microenvironment in vitro [25]. The same technique has been used by Wang et al. to build hydrogel microfibers with glioma stem cell GSC23 in the shell and glioma cell line U118 in the core [26]. They arranged a series of drug resistance experiments on different microfibers and confirmed that the microfiber could also be a valuable tool for drug development and screening. Also, a patient-specific glioblastoma-on-a-chip with centric hypoxia was built by Yi et al. [27] to reproduce clinically observed patient-specific resistances to treatment with concurrent chemoradiation and temozolomide and the model could be used to determine drug combinations associated with superior tumor killing. Different from brain tumor bioprinting, Han and Hsu [28] put forward a potential strategy using bioinks mixed with neural–vascular spheroids to generate mini-brain constructs as research tools and neural grafts. All these models mentioned above are capable of the investigation of interactions of different cell types and environmental factors, and they could be used for clinical research to find more effective treatments for diverse tumors and diseases. However, most of these models mainly focus on the tumor cells themselves and not pay too much attention to their ECM microenvironments, so they cannot faithfully reproduce the disease model in vivo. Thus, it is a primary task to fabricate in vitro brain microenvironment model by 3D bioprinting techniques for brain tumor study. It is well established that the dominant component of the human brain is glial cells accounting for 72% of the tissue volume and 90% of the cell volume in the brain. And normal brain contains 20% of the ECM and the dominant composition is Hyaluronic acid (HA).

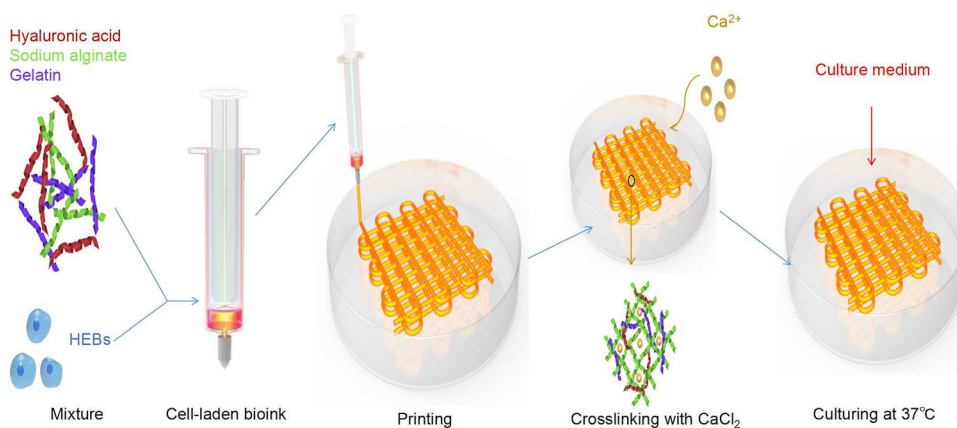
In this study, we adapted a pneumatic extrusion 3D bioprinting system to build available structures of the matrices to construct the brain matrix-mimetic microenvironment model with human glial cells mixed within the HA-based bioinks (Fig. 1). We investigated the formulation of bioinks and the impacts of gelatin (GA) on the mechanical and biological properties of the brain matrix-mimetic microenvironment models with different scaffolds. We verified the differences of the performances of models with multiple experiments and proved that the bioprinted brain matrix-mimetic microenvironment model could mimic the in vivo GBM stroma environment to a certain degree and could be used as a reliable platform to co-culture diverse cell types and study the biological behaviors of GBM in the future.

Materials and methods

Bioink formulation

The hyaluronic acid powder (XIYA Reagent, Shandong, China), sodium alginate powder (Sinopharm Chemical Reagent Co., Ltd., Shanghai, China), gelatin powder

Fig. 1 Schematic of the 3D cell-laden scaffold printing process



(Sigma-Aldrich, Shanghai, China) and calcium chloride (CaCl_2) powder (Sigma-Aldrich, Shanghai, China) were sterilized under ultraviolet (UV) light for 2 h. The concentration of HA was between 0.005 and 0.02 g/ml, the concentration of SA was between 0.01 and 0.02 g/ml, and the concentration of GA was between 0 and 0.1 g/ml according to a different formulation of the bioinks for the following research. The powders were dissolved in deionized water at 50 °C, and the mixture was blended and stirred for 30 min at 200 r/min to be homogeneous. Bioinks with different formulations of these components were sealed and labeled in centrifuge tubes and stored at 4 °C. CaCl_2 solution with a concentration of 0.05 g/ml was also prepared for cross-linking.

Model design

Here, we adapted two most common structures of the model, one is multilayered grid matrix and the other is monolayered solid membrane, both of which are relatively simple to print and convenient for observation of cells in the scaffold and could provide sufficient superficial area for the exchange of substance with the culture medium.

Optimization of the printing process

The formulation and concentration of different components of the bioink would strongly affect the mechanical properties of the model such as the stiffness, viscosity and porosity, so the printability and formability of the matrices depended a lot on the formulation of the bioink. In the meantime, the regulation of the controllable parameters in the printing process also had a great influence on the modeling, such as the type and length of the nozzle, extrusion pressure, the speed of nozzle movement and the change of temperature, all of which would influence the diameter of the extrusion line width. Besides, various parameters such as line spacing and the layer spacing could also lead to different printing effects. So, we had to strictly control the influence of these factors

and conducted several reasonable gradient experiments to find out the best combination range of bioinks and optimized printing process and parameters. It is worth emphasizing that although all of those variables and parameters mentioned previously would have certain influence on the effect of printing, only a few of them were necessary to be taken into consideration when designing the experiments because the influence of most variables were controllable and predictable. The aim of the experimental setup in this section is to efficiently find out available ranges of bioink components as well as the printing conditions. So it is required to adjust multiple parameters with range partition formulations of bioinks in the same time.

Stiffness test

In order to simulate the microenvironment of human brain tissue *in vivo*, the stiffness of the bioprinted scaffold of the model was expected to be as close to the stiffness of human brain tissue as possible. Hence, stress–strain measurements were carried out using a uniaxial loading with a range of 20 N at room temperature delivered by an Electro Force Universal Testing Machine (TA Instruments, New Castle DE, USA). Here, the nominal tensile modulus was used as a horizontal standard to compare the stiffness of models with different concentrations of gelatin within the bioinks and the samples were casted to be the standard dumbbell-shaped specimens with uniform cross section (width 2 mm, thickness 2 mm) and initial stretch length of 4 mm.

Scanning electron microscopy (SEM)

SEM sample preparation and imaging were performed to observe the microcellular structure of the hydrogel with different concentration of gelatin to compare the morphology and microstructure formation of the scaffold using a scanning electron microscope (SEM; JEM-6700F, JEOL Co., Ltd., Tokyo, Japan) at the 5th day of culturing after

printing. For SEM images, the samples were lyophilized and cut into smaller specimens (about 2 mm × 2 mm) attached to carbon tape. Then, the specimens were sputter-coated with a thin layer of electrically conducting material on the surface. Micrographs of the coated specimens were taken under vacuum conditions.

Cell culture

Human glial cell (HEB) was cultured in Dulbecco's modified Eagle medium/nutrient mixture F-12 (DMEM/ F12; Gibco, Carlsbad, CA, USA) supplemented with 10% fetal bovine serum (FBS) and incubated in polystyrene tissue culture flasks at 37 °C in 5% CO₂, fed with fresh culture medium every day and passaged every other day. HEBs were used to mix within the hydrogel to fabricate cell-laden bioinks to investigate the biological properties of the brain microenvironment simulation model such as cell viability and proliferation. HEBs were exposed to trypsin–ethylenediaminetetraacetic acid (EDTA) solution (0.25%:0.02%) for 3 min at 37 °C in 5% CO₂ after washed with phosphate-buffered saline (PBS) and then centrifuged at 1000 r/min for 5 min. The cells were then suspended in the hydrogel to a concentration of 1.5×10^6 cells/ml.

Cell viability assay

Cell survival rates in different structures of models with different concentrations of gelatin were measured and compared at days 1, 7 and 14 after printing using LIVE/DEAD™ Viability/Cytotoxicity Kit (Invitrogen). The images of live/dead cells were taken by stereo-fluorescence microscope (Olympus, Beijing, China) and processed with ImageJ to calculate the averaged cell survival rates in multiple fields and samples.

Cell proliferation assay

The cell proliferation performance in different structures of models with different concentrations of gelatin was measured and compared every other day for 14 days after printing using Cell Counting Kit-8 (MedChem Express). To compare the cell proliferation rate in different models with a different initial number of cells, the initial number of cells of all the tested groups was all set to be 1 and the greatest number of cells was all set to be 2 in order to use the proliferation ratio of the same groups for more intuitional comparison.

Histological analysis and fluorescence microscopy

In order to evaluate cell adhesion and spreading in the scaffold, the cell-laden matrices were prepared and processed on the 5th day of culturing after printing. Hematoxylin–eosin

staining was used to observe the microstructure of the scaffold and the morphology of HEBs in the bioink. Immunofluorescence imaging of vinculin (green), F-actin (red) and nuclear DNA (blue) was conducted to investigate the cell adhesion and morphology in scaffolds of the model with different concentrations of gelatin. Morphometric analyses of the cell area and circularity among three types of bioinks were conducted by processing the immunofluorescence images to define the cell boundaries and applying particle analysis automatically in ImageJ, and the circularity was described as $4\pi \times \text{area}/\text{perimeter}^2$ which means 0 for a straight line and 1 for a circle.

Data analysis and statistics

The stiffness and biocompatibility assay data were obtained from two or more independent samples, each measured or calculated in duplicate. Significance analyses among data sets with homogeneity of variance (cell area) were determined using one-way ANOVA followed by Bonferroni post hoc test for multiple comparisons. Significance analyses among data sets with heterogeneity of variance (stiffness, cell survival rate and circularity) were determined using one-way ANOVA followed by Games–Howell post hoc test for multiple comparisons. In both cases, statistically significant differences among discrete groups were indicated on graphs by asterisks (*for $p < 0.05$, **for $p < 0.01$ and *** for $p < 0.001$).

Results and discussion

Printability assay

Hyaluronic acid (HA) is one of the major components of the extracellular matrix (ECM) of the brain and is characterized by excellent natural biocompatibility and indispensability in regulating cellular behaviors [29–31]. In addition, it plays a significant role in tumor progression and invasion [32]; hence, it is chosen to be one of the key components of the bioink in this study. However, few research works have been done with HA-based bioink for 3D bioprinting due to its high viscosity and poor post-printing shape stability [33]. Thus, the HA-based bioink in microextrusion bioprinting is obliged to be modified or combined with other types of biomaterials. Since alginate-based bioinks are found to be satisfying in cell encapsulation and survival, and some of other modified materials would bring about the difficulty in removal of cross-linking agents and cytotoxicity, we used physical cross-linking strategy through sodium alginate(SA) and calcium chloride(CaCl₂) solution and intended to add gelatin(GA) into the bioink for its excellent biocompatibility

and help to maintain stable form of the printed models under high load and deformation during the printing process.

The difference in the concentration of the three types of materials will lead to the difference in mechanical properties of the model such as printability, formability and stability, affecting the availability and the life period of the printed model. In the meantime, the regulation of the controllable parameters in the printing process also has a great influence on the modeling, such as the material and shape of the nozzle, extrusion pressure, the length and diameter of the cylinder, the speed of nozzle movement and the change of temperature, all of which would influence the diameter of the extrusion line width of the printed scaffold. There are also various parameters such as the line spacing and layer spacing that could lead to different printing effects. So, we need to set a series of reasonable gradient experiments for multiple factors to find out the available combination of the printing parameters with the range of the concentration of printed materials to optimize the printing process. Although it seems complicated to design the experimental setup considering multiple variables as well as the uncertain concentration of the bioinks all together at the same time, it is obvious that we could not adjust these variables exhaustively to figure out a determined value in view of time and efficiency. In fact, only a few essential parameters are required to be investigated specifically in the experiments such as the extrusion pressure and the line spacing. The rest of the printing parameters could be adjusted accordingly during the experiments because the influences of them on the printing effect are generally predictable and controllable. Regarding the concentration of the bioink compositions, there are also ways to define the suitable range of concentration of the bioink at high efficiency. The compositions of the bioink are settled to be HA, SA and GA as mentioned previously; therefore, several extremums and test values of these materials could be set according to their physiochemical properties such as solubility and kinetics as well as their biocompatibility. It needs to be pointed out that the target of these experiments in this section is to figure out available ranges of bioink formulations with appropriate printing conditions, rather than investigating the determined values of all the printing variables thoroughly at the same time. In addition, since the macrostructure of the scaffold is of a little amount of importance compared with the microstructure in this study, we only take printability, formability and stability into consideration when it comes to the assessment of the printing effect in this section. The printability mainly depends on the viscosity of the bioink and the range of extrusion pressure. As for the formability, the factors taken into account include the clear hierarchy or layered structure of the scaffold and homogeneity of the extruded fiber. The stability means that the models we printed have to maintain stable shape and structure during and after printing for 14 days at

a cell incubation environment without melting, collapsing, or rupturing. To study the optimized combination of printing parameters and the proper range of bioink concentration, only two variables were investigated at the same time when other variables were adjusted accordingly (Fig. 2).

For the pneumatic extrusion bioprinting system that we have adopted in this study, the diameter of the extrusion line width tends to increase as the extrusion pressure and the diameter of the nozzle increase and decrease as the length and movement speed of the nozzle increase. At the same time, the temperature of both the nozzle and the cylinder affects the viscosity of the bioink and the temperature of the platform affects the stability of the model under printing, thus affecting the extrusion pressure and the distance between adjacent fibers required. During the experiment, the movement speed of nozzle was generally taken the default value of 2.3 units/sec, and the type of the nozzle was fixed to be 25G with an inner diameter of 0.26 mm, an external diameter of 0.51 mm and a length of 25 mm. The temperature of the nozzle and cylinder was set to be 37 °C to guarantee the viability of the cells in the bioink, and the temperature of the platform was set to be 4 °C for solidification of the gelatin. Besides, the distance and speed of the rise of the nozzle and standing time between two adjacent layers when printing a multilayered structure would also affect the printing effect. So during the experiments, we need to strictly control the influence of these factors accordingly. After a series of gradient experiments, the concentration of HA and SA was fixed to be 0.015 g/ml, and the concentration of GA was set to be a gradient of 0, 0.0375 g/ml and 0.075 g/ml. The printing parameters were adjusted according to the formulation of bioinks. The models printed in this study showed a clearly layered structure and coherent line width during the printing process and were able to maintain stable shape and architecture for 14 days immersed in culture medium and cultured in the cell incubator at 37 °C without melting, collapsing, or rupturing, providing available and basic conditions for various biological experiments following.

Stiffness comparison

In this study, the concentration of calcium chloride (CaCl_2) solution for the cross-linking process was chosen to be 0.05 g/ml. We named three types of bioink with different concentrations of gelatin to be type A—0.015 g/ml HA, 0.015 g/ml SA; B—0.015 g/ml HA, 0.015 g/ml SA and 0.0375 g/ml GA; and C—0.015 g/ml HA, 0.015 g/ml SA and 0.075 g/ml GA. The standard dumbbell-shaped samples were cross-linked with 0.05 g/ml CaCl_2 solution by immersing in it right after printing for 3 min and then rinsed with phosphate-buffered saline (PBS). The stiffness of human brain tissue varies with region, age, tropism and measurement methods such as magnetic resonance elastography

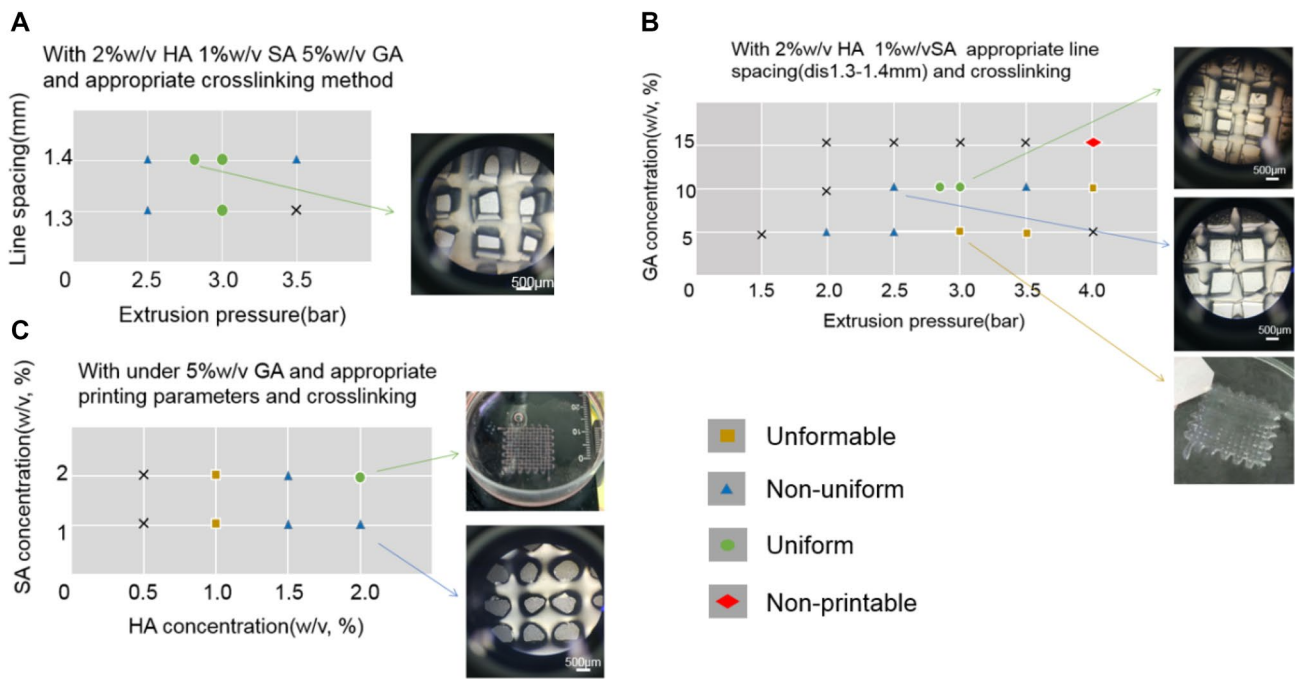


Fig. 2 Optimization of the printing process. **a** Exploration of the extrusion pressure and line spacing with a fixed concentration of bioinks. **b** The relationship between the concentration of gelatin and

the extrusion pressure. **c** Investigation of the range of concentration with hyaluronic acid and sodium alginate

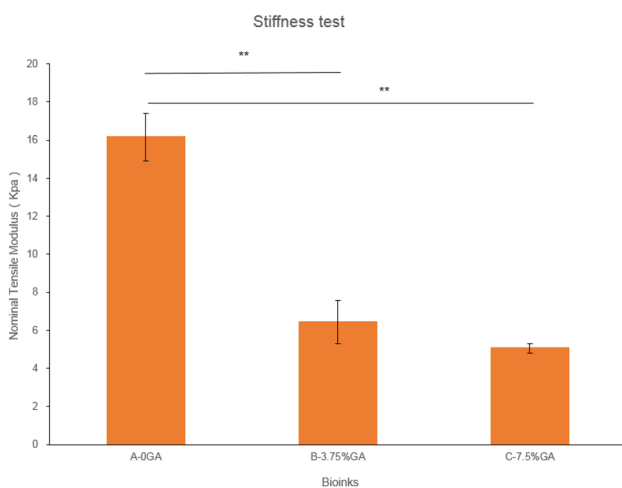


Fig. 3 Nominal tensile modulus of dumbbell-shaped samples with type A, B and C bioinks

(MRE), magnetic resonance imaging (MRI) and atomic force microscope (AFM) and the typical order of magnitude ranges from 10^2 to 10^3 Pa, which affects the cell behavior largely and should be mimicked as closely as possible [34–40]. It was suggested that the higher concentration of gelatin in these three types of bioink, the softer materials performed in standard dumbbell-shaped models (Fig. 3), which meant the models printed with type C bioink with

7.5%w/v of gelatin had the most close stiffness to that of human brain tissue among all the tested groups which were on the same order of magnitude due to the liquefied and loss of gelatin when the models were cultured at 37 °C and the porous structure was formed inside the hydrogel. Although it could be noticed that the stiffness of optimized cross-linked bioink chosen as type C bioink as mentioned was still higher than that of cerebral tissue in vivo, it was relatively tolerable in this study considering the viscosity requirements of our extrusion-based bioprinting platform for the bioink as well as the demand for mechanical formability and stability of the model.

Biocompatibility assay

In order to observe the viability of HEBs in scaffolds with different structures and bioinks, we tested the cell survival rate separately at days 1, 7 and 14 to compare the impact of gelatin and the influence of the two structures of the matrices on cell viability (Fig. 4a–d). Also, the proliferation rate was taken into consideration. The number of tested groups in these two experiments above was supposed to be 6, respectively, permuted and combined with three types of materials and two types of structures of the models. However, it is difficult for type A bioink with only hyaluronic acid and sodium alginate to print multilayered grid scaffold without collapse or fusion of the extrusion

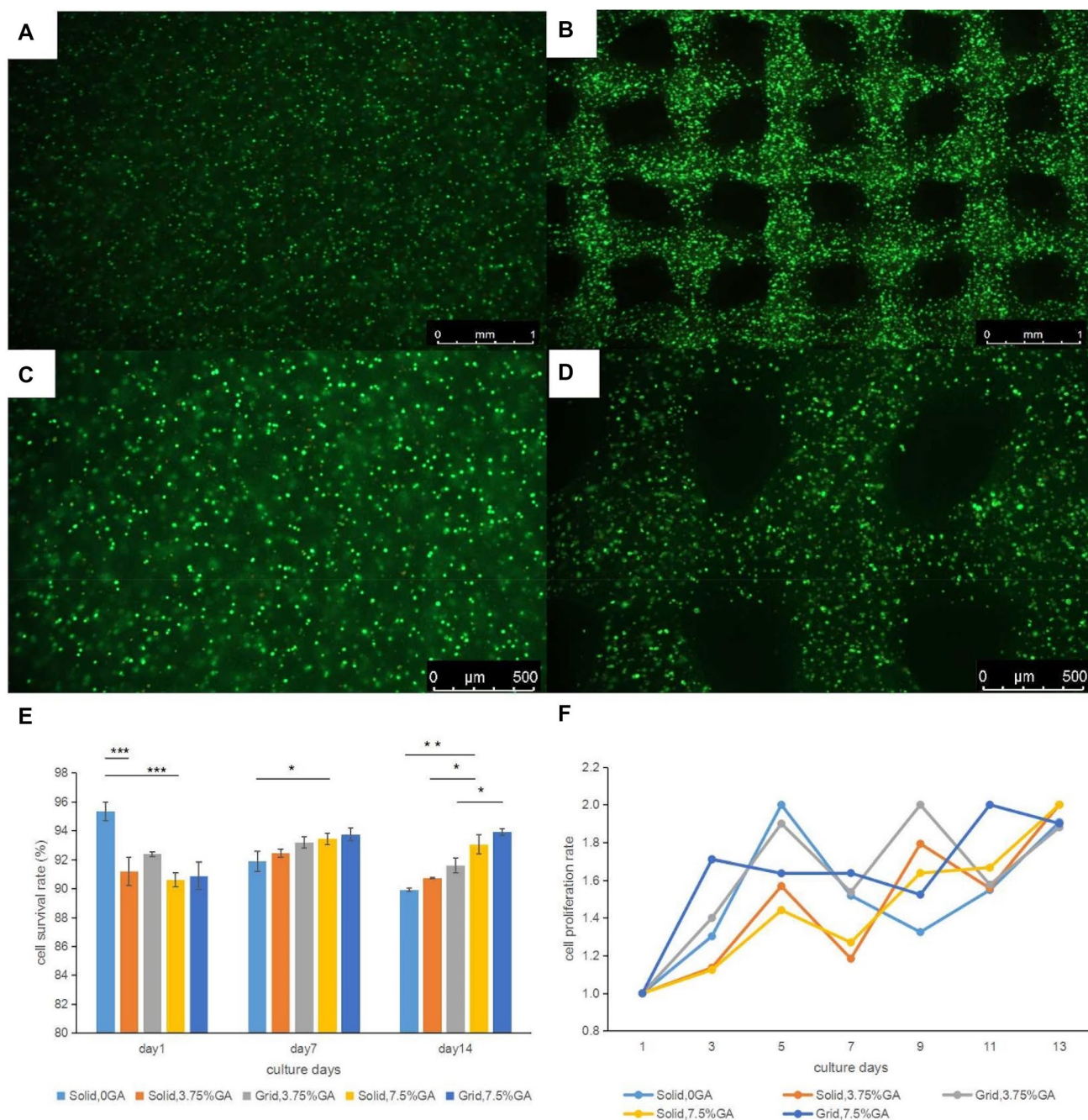


Fig. 4 Live/dead stain of HEBs at day 1 after printing in **a** monolayered solid membrane and **b** multilayered grid model (scale bar: 1 mm); **c** monolayered solid membrane and **d** multilayered grid

model (scale bar: 500 μ m); **e** cell survival rate in five tested groups at day 1, 7 and 14 after printing; **f** cell proliferation rate in five tested groups during 14 days of culture

fibers of the model during the printing process due to the lack of gelatin support and poor formability, so in this study, the cell survival rate and proliferation rate were only compared among five tested groups: bioink A of monolayered solid membrane model, bioink B of both monolayered solid structure and multilayered grid model, and bioink C of both monolayered solid structure and multilayered

grid model. It turned out that appropriate concentration of gelatin and the multilayered grid scaffolds have a limited improvement in cell viability compared with bioinks without gelatin and printed to be solid membrane structure in long-term culture because of the increased surface area of those models for the acquisition of nutrients and oxygen in the culture medium and the improved biocompatibility

by gelatin (Fig. 4e). But overall the cell viability and proliferation in all tested groups showed relatively satisfying outcomes and the cell survival rate remained over 85% even after 14 days of culture (Fig. 4e, f).

For further investigation of the microstructure of A, B and C bioinks along with the cell morphology within the scaffolds, SEM images were taken to investigate and compare the formation of porous structures of the bioinks (Fig. 5a–c) and histological hematoxylin–eosin (H&E) staining was used to observe the morphology of HEBs in the bioink (Fig. 5d–f). It was revealed that when the bioink did not contain gelatin and only consisted of hyaluronic acid and sodium alginate, the hydrogel was formed with sheet-like structures and showed a denser architecture (Fig. 5a). The HEBs within the scaffold showed tight adhesion and junction (Fig. 5d). With the increase in the concentration of gelatin after culturing at 37 °C for several days, the microstructure of the hydrogel became more porous and reticular (Fig. 5b, c). And the cells within the scaffolds showed a more dispersed distribution and located along with the direction of the reticular fibers formed in the microstructure (Fig. 5e, f), which could also give an explanation from a certain point of view to the improved cell viability in type B and C bioinks previously mentioned. Also, it is assumed that cells tend to get better motility in hydrogels with a more porous structure or lower stiffness, so the morphometric analyses of the HEBs in different bioinks should also be carried out for further investigation of the cell adhesion, spreading, migration and aggregation.

To further investigate the cellular behaviors especially the morphology alteration inside the hydrogels with different formulations of bioinks, immunofluorescence assay was taken. In this study, we stained nuclear area with DAPI shown in blue and cell–skeleton with F-actin shown in red and cell–ECM interaction with VINCULIN shown in green. As a further illustration of the cell morphology in three types of materials with different concentration of gelatin and stiffness agreed with the observation in hematoxylin–eosin staining, it was obvious that HEBs in type A bioink with the sheet-like microstructures exhibited applanate forms and adhered to the layered and expanded fibers, showing relatively low circularity and irregular shapes (Fig. 6a–d). Nevertheless, with the increase in gelatin and decreasing of the stiffness of the bioink, the cells in type B bioink tented to perform rounded morphologies and increased circularity (Fig. 6e–h) which indicated less adhesion to the microfibers of the scaffold. Moreover, when the stiffness of the bioink further declined and became proximate to the human brain tissue *in vivo* along with distinct porous structure and reticular microfibers formed in the scaffold, the cells in type C bioink exhibited more extensional morphologies with elongated synaptic structures, decreased circularity and some of the cells even aggregated to form clusters (Fig. 6i–l), which indicated enhanced abilities of stretching and mobility. In addition, cells in type C bioink with 7.5%w/v of gelatin also showed elongated vinculin-positive focal spreading, actin-based stress fibers and more pseudopodium compared with the adhered morphology of cells in type A bioink and the

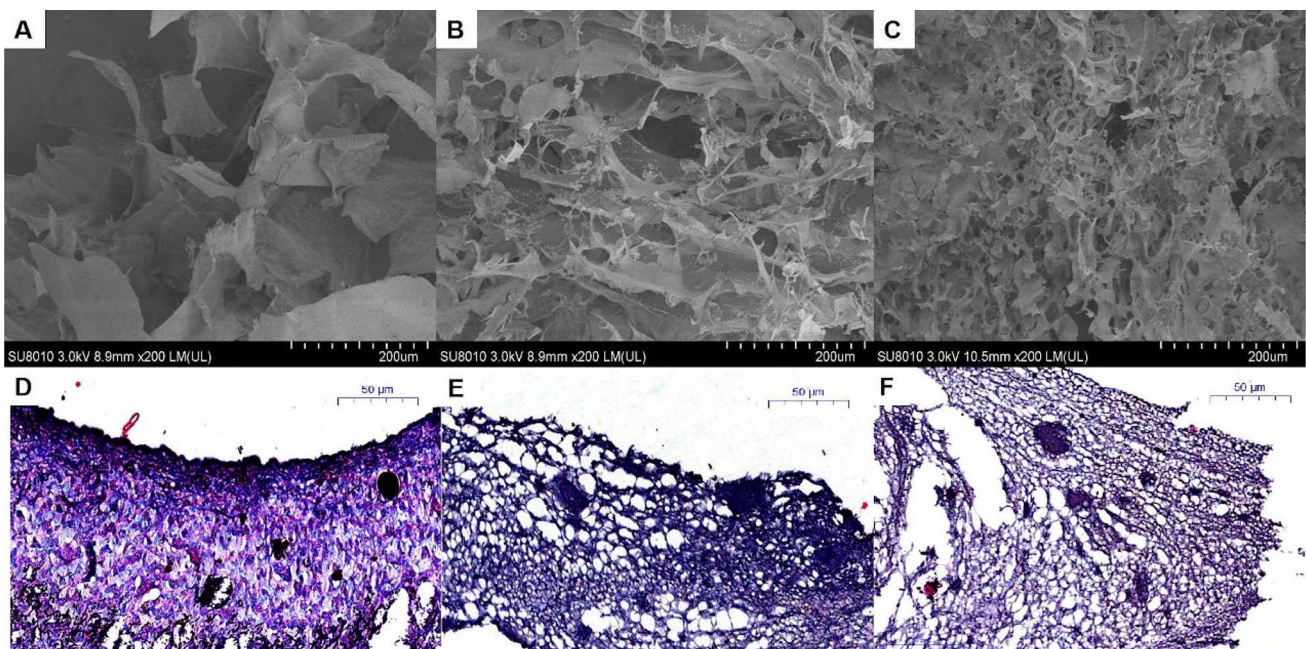


Fig. 5 a–c Scanning electron microscopy (SEM) imaging of type A, B and C bioinks (scale bar: 200 μm). d–f Hematoxylin–eosin staining of HEBs within types A, B and C bioinks (scale bar: 50 μm)

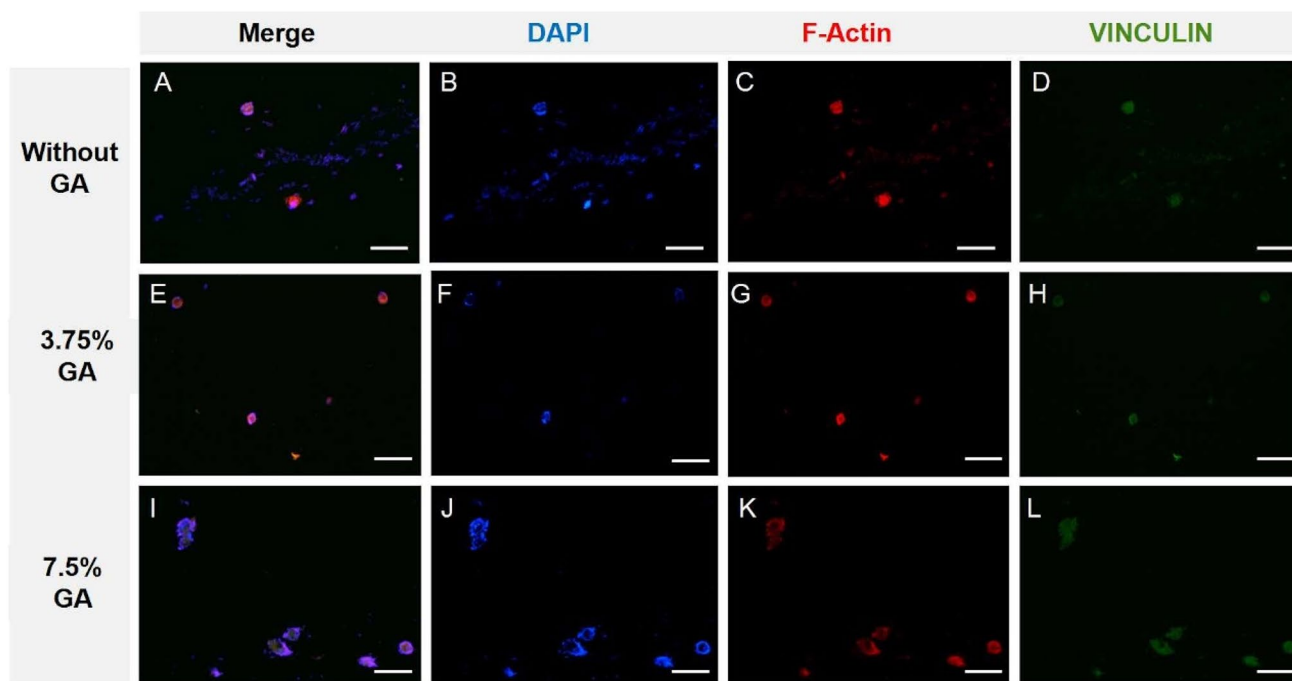


Fig. 6 Immunofluorescence imaging of HEB cells in the printed samples with vinculin (green), F-actin (red) and nuclear DNA (blue) in three formulations of bioinks. **a–d** without GA, **e–h** 3.75% GA, **i–l** 7.5% GA (scale bar: 50 μm)

rounded morphology of cells in type B bioink. In the cell area and cell circularity test, we can be based on the results and analyses above, the formulation of type C bioink is expected to be applied as a good candidate bioink to print brain tumor models and study the biological features including invasion progress of GBM tumor cells in the following research in the future (Fig. 7).

The *in vitro* brain microenvironment model bioprinted in this study promises an available platform for GBM invasion study in the future. In the next step, we will seed pre-formed GBM microtumors with hanging drop methods onto the above printed brain matrix-mimetic and investigate the

co-culture of glial cells (HEB) and GBM cells (U87). We will add chemoattractant such as glucose to induce the GBM cell invasion. It is well established that glucose can induce breast cancer cell MDA-MB-231 invasion inside the 3D collagen hydrogel matrix [41]. Some preliminary 2D culture results have shown that with the HEB cells the GBM cells tend to form more sphere-like structure in the 2D co-cultures that means the HEB cells and their microenvironments can significantly change the GBM cellular behavior. Furthermore, we will explore the gene and protein expression difference before and after GBM invasion with genomic and proteomics approaches and identified the genes and proteins

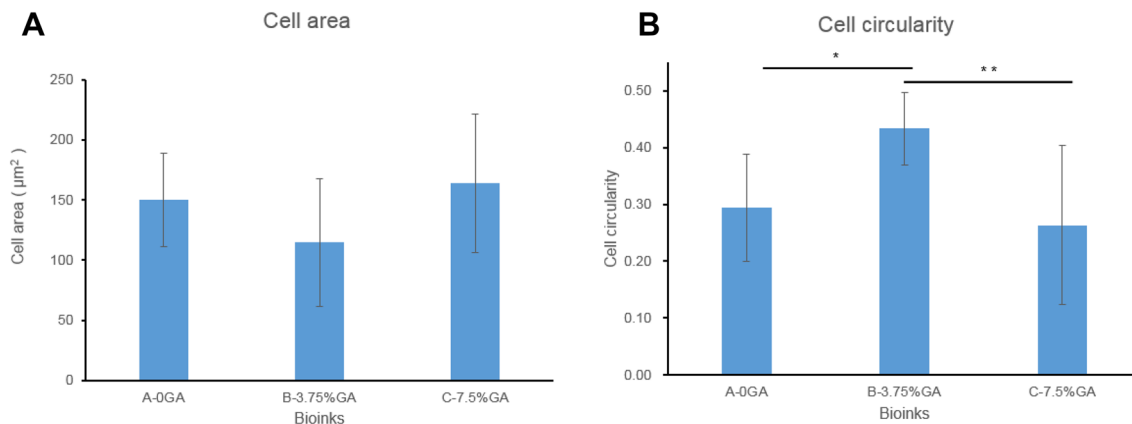


Fig. 7 **a** Cell area and **b** cell circularity between different formulations of bioinks

which may take important roles during GBM invasion. We have demonstrated that the GBM cell cultured in 2D and 3D have significantly gene alternations [42]. We hope this 3D printed HA-based brain matrix-mimetic GBM invasion model can be a powerful platform to mimic the GBM invasion in vitro to enhance our understanding of the molecular level and potential to be an effective tool for anticancer drug screening.

Conclusion

This study focused on the construction of brain matrix-mimetic as human brain microenvironment with 3D extrusion-based bioprinting. The formulation of the bioink was discussed, and the effect of gelatin within the hydrogel was studied through the comparison of both mechanical and biological properties of the model to mimic the microenvironment of brain tissue in vivo. We also optimized the printing process and investigated the influence of scaffold structure on the behaviors of normal glial cell HEB with diverse experiments. We demonstrated that bioinks with a certain range of gelatin could exhibit lower stiffness which was relatively close to human brain tissue and porous fiber-like microstructures which promotes cell viability, aggregation and motility. This brain matrix-mimetic microenvironment model was anticipated to be adapted to GBM invasion mechanism study and drug screening; also the model was able to provide a versatile platform to study multiple cells interaction and other biological environments.

Acknowledgements We would like to thank the support by the National Key Research and Development Program of China (2018YFA0703000), National Natural Science Foundation of China (Grant No. 51875518), Key Research and Development Projects of Zhejiang Province (Grant No. 2017C01054 and No. 2018C03062) and the Fundamental Research Funds for the Central Universities (Grant No. 2019XZZX003-02, 2019FZA4002).

Compliance with ethical standards

Conflict of interest The authors declare that there is no conflict of interest.

Ethical approval This study does not contain any studies with human or animal subjects performed by any of the authors.

References

- Rao SS, Lannutti JJ, Viapiano MS, Sarkar A, Winter JO (2014) Toward 3D biomimetic models to understand the behavior of glioblastoma multiforme cells. *Tissue Eng Part B Rev* 20:314–327
- Kirkpatrick JP, Laack NN, Shih HA, Gondi V (2017) Management of GBM: a problem of local recurrence. *J Neurooncol* 134:487–493
- Wang K, Florczyk S, Kievit F, Zhang MQ (2014) Culture of human GBM cells on ECM-mimicking chitosan-hyaluronic acid scaffolds increases malignancy and drug resistance. *Neuro-Oncol* 16:v124
- Florczyk SJ, Wang K, Jana S, Wood DL, Sytsma SK, Sham J, Kievit FM, Zhang M (2013) Porous chitosan-hyaluronic acid scaffolds as a mimic of glioblastoma microenvironment ECM. *Biomaterials* 34:10143–10150
- Stock K, Estrada MF, Vidic S, Gjerde K, Rudisch A, Santo VE, Barbier M, Blom S, Arundkar SC, Selvam I, Osswald A, Stein Y, Gruenewald S, Brito C, Van Weerden W, Rotter V, Boghaert E, Oren M, Sommergruber W, Chong Y, De Hoogt R, Graeser R (2016) Capturing tumor complexity in vitro: comparative analysis of 2D and 3D tumor models for drug discovery. *Sci Rep* 6:28951
- Rodenhizer D, Dean T, D'arcangelo E, Mcguigan AP (2018) The current landscape of 3D in vitro tumor models: what cancer hallmarks are accessible for drug discovery? *Adv Healthc Mater* 7:e1701174
- Ferreira LP, Gaspar VM, Mano JF (2018) Design of spherically structured 3D in vitro tumor models -Advances and prospects. *Acta Biomater* 75:11–34
- Tsai CW, Wang JH, Young TH (2018) Core/shell multicellular spheroids on chitosan as in vitro 3D coculture tumor models. *Artif Cells Nanomed Biotechnol* 46:S651–S660
- Pang Y, Mao SS, Yao R, He JY, Zhou ZZ, Feng L, Zhang KT, Cheng SJ, Sun W (2018) TGF-beta induced epithelial-mesenchymal transition in an advanced cervical tumor model by 3D printing. *Biofabrication* 10:044102
- Santo VE, Rebelo SP, Estrada MF, Alves PM, Boghaert E, Brito C (2017) Drug screening in 3D in vitro tumor models: overcoming current pitfalls of efficacy read-outs. *Biotechnol J* 12
- Nunes AS, Barros AS, Costa EC, Moreira AF, Correia IJ (2019) 3D tumor spheroids as in vitro models to mimic in vivo human solid tumors resistance to therapeutic drugs. *Biotechnol Bioeng* 116:206–226
- Ma L, Barker J, Zhou C, Li W, Zhang J, Lin B, Foltz G, Kublbeck J, Honkakoski P (2012) Towards personalized medicine with a three-dimensional micro-scale perfusion-based two-chamber tissue model system. *Biomaterials* 33:4353–4361
- Gill EL, Li X, Birch MA, Huang YYS (2018) Multi-length scale bioprinting towards simulating microenvironmental cues. *Bio-Des Manuf* 1:77–88
- Zhang B, Luo YC, Ma L, Gao L, Li YT, Xue Q, Yang HY, Cui ZF (2018) 3D bioprinting: an emerging technology full of opportunities and challenges. *Bio-Des Manuf* 1:2–13
- Jian HL, Wang MY, Wang ST, Wang AH, Bai S (2018) 3D bioprinting for cell culture and tissue fabrication. *Bio-Des Manuf* 1:45–61
- Wang X, Zhang X, Dai X, Wang X, Li X, Diao J, Xu T (2018) Tumor-like lung cancer model based on 3D bioprinting. *3 Biotechnology* 8:501
- Zahedi-Tabar Z, Bagheri-Khoulenjani S, Mirzadeh H, Amanpour S (2019) 3D in vitro cancerous tumor models: using 3D printers. *Med Hypotheses* 124:91–94
- Zhang B, Gao L, Ma L, Luo YC, Yang HY, Cui ZF (2019) 3D Bioprinting: a novel avenue for manufacturing tissues and organs. *Engineering* 5:777–794
- Albritton JL, Miller JS (2017) 3D bioprinting: improving in vitro models of metastasis with heterogeneous tumor microenvironments. *Dis Model Mech* 10:3–14
- Ma H, Luo J, Sun Z, Xia L, Shi M, Liu M, Chang J, Wu C (2016) 3D printing of biomaterials with mussel-inspired nanostructures for tumor therapy and tissue regeneration. *Biomaterials* 111:138–148

21. Zhang YS, Duchamp M, Oklu R, Ellisen LW, Langer R, Khademhosseini A (2016) Bioprinting the cancer microenvironment. *ACS Biomater Sci Eng* 2:1710–1721
22. Choi YR, Kim JH, Park SJ, Hur BY, Han JK (2017) Therapeutic response assessment using 3D ultrasound for hepatic metastasis from colorectal cancer: application of a personalized, 3D-printed tumor model using CT images. *PLoS ONE* 12:e0182596
23. Heinrich MA, Bansal R, Lammers T, Zhang YS, Michel Schiffelers R, Prakash J (2019) 3D-bioprinted mini-brain: a glioblastoma model to study cellular interactions and therapeutics. *Adv Mater* 31:e1806590
24. Dai X, Ma C, Lan Q, Xu T (2016) 3D bioprinted glioma stem cells for brain tumor model and applications of drug susceptibility. *Biofabrication* 8:045005
25. Dai X, Liu L, Ouyang J, Li X, Zhang X, Lan Q, Xu T (2017) Coaxial 3D bioprinting of self-assembled multicellular heterogeneous tumor fibers. *Sci Rep* 7:1457
26. Wang X, Li X, Dai X, Zhang X, Zhang J, Xu T, Lan Q (2018) Coaxial extrusion bioprinted shell-core hydrogel microfibers mimic glioma microenvironment and enhance the drug resistance of cancer cells. *Colloids Surf B Biointerfaces* 171:291–299
27. Yi HG, Jeong YH, Kim Y, Choi YJ, Moon HE, Park SH, Kang KS, Bae M, Jang J, Youn H, Paek SH, Cho DW (2019) A bio-printed human-glioblastoma-on-a-chip for the identification of patient-specific responses to chemoradiotherapy. *Nat Biomed Eng* 3:509–519
28. Han HW, Hsu SH (2017) Using 3D bioprinting to produce mini-brain. *Neural Regen Res* 12:1595–1596
29. Stratesteffen H, Kopf M, Kreimendahl F, Blaeser A, Jockenhoevel S, Fischer H (2017) GelMA-collagen blends enable drop-on-demand 3D printability and promote angiogenesis. *Biofabrication* 9:045002
30. Das D, Pham TTH, Noh I (2018) Characterizations of hyaluronate-based terpolymeric hydrogel synthesized via free radical polymerization mechanism for biomedical applications. *Colloid Surf B* 170:64–75
31. Highley CB, Prestwich GD, Burdick JA (2016) Recent advances in hyaluronic acid hydrogels for biomedical applications. *Curr Opin Biotechnol* 40:35–40
32. Ananthanarayanan B, Kim Y, Kumar S (2011) Elucidating the mechanobiology of malignant brain tumors using a brain matrix-mimetic hyaluronic acid hydrogel platform. *Biomaterials* 32:7913–7923
33. Noh I, Kim N, Tran HN, Lee J, Lee C (2019) 3D printable hyaluronic acid-based hydrogel for its potential application as a bioink in tissue engineering. *Biomater Res* 23:3
34. Engler AJ, Sen S, Sweeney HL, Discher DE (2006) Matrix elasticity directs stem cell lineage specification. *Cell* 126:677–689
35. Flanagan LA, Ju YE, Marg B, Osterfield M, Janmey PA (2002) Neurite branching on deformable substrates. *NeuroReport* 13:2411–2415
36. Iwashita M, Kataoka N, Toida K, Kosodo Y (2014) Systematic profiling of spatiotemporal tissue and cellular stiffness in the developing brain. *Development* 141:3793–3798
37. Iwashita M, Ohta H, Fujisawa T, Cho M, Ikeya M, Kidoaki S, Kosodo Y (2019) Brain-stiffness-mimicking tilapia collagen gel promotes the induction of dorsal cortical neurons from human pluripotent stem cells. *Sci Rep* 9:3068
38. Kalra P, Raterman B, Mo X, Kolipaka A (2019) Magnetic resonance elastography of brain: comparison between anisotropic and isotropic stiffness and its correlation to age. *Magn Reson Med* 82:671–679
39. Takamura T, Motosugi U, Sasaki Y, Kakegawa T, Sato K, Glaser KJ, Ehman RL, Onishi H (2019) Influence of age on global and regional brain stiffness in young and middle-aged adults. *J Magn Reson Imaging* 51:727–733
40. Yang Y, Wang K, Gu X, Leong KW (2017) Biophysical regulation of cell behavior-cross talk between substrate stiffness and nanotopography. *Engineering (Beijing)* 3:36–54
41. Liu LY, Duclos G, Sun B, Lee J, Wu A, Kam Y, Sontag ED, Stone HA, Sturm JC, Gatenby RA, Austin RH (2013) Minimization of thermodynamic costs in cancer cell invasion. *Proc Natl Acad Sci USA* 110:1686–1691
42. Ma L, Zhang B, Zhou C, Li Y, Li B, Yu M, Luo Y, Gao L, Zhang D, Xue Q, Qiu Q, Lin B, Zou J, Yang H (2018) The comparison genomics analysis with glioblastoma multiforme (GBM) cells under 3D and 2D cell culture conditions. *Colloids Surf B Biointerfaces* 172:665–673